Kinematics Analysis and Simulation of Mobile Robot Based on Linkage Suspension

Ya Chen*1, Dianjun Wang*†1, Haoxiang Zhong*1, Yadong Zhu*1, and Chaoxing Wang*2

*1Beijing Institute of Petrochemical Technology, No.19 Qingyuan North Street, Huangcun Town, DaxingDistrict, Beijing, 102617, China
E-mail: chenya@bipt.edu.cn, wangdianjun@bipt.edu.cn, zhonghaoxiang@bipt.edu.cn, zhuyadong@bipt.edu.cn
*2Beijing U-precision Tech Co., Ltd, NO.19 Kechuang 10th Street, BDA, Daxing District, Beijing, 100176, China
E-mail: 867023046@qq.com
†Corresponding author

Abstract. The complex kinematics modeling of mobile robot with connecting rod suspension is studied. According to the wheel center modeling method, the kinematic characteristics of the six wheels of the mobile robot under irregular terrain are analyzed and the kinematics theoretical model is established. Then, the kinematics simulation analysis is carried out through the virtual prototype technology to verify the rationality of structural design and the correctness of the kinematics theoretical model. Finally, the error test of the mobile robot prototype is executed, the minimum deviation error of the linear motion is 4.399mm, the forward and backward in-situ turning error is 1.166mm and 0.838mm, respectively. The test results show that the kinematics theoretical analysis of the mobile robot is reasonable, the robot has good motion ability. The study provides a theoretical basis for the research of high-quality navigation and control system of the mobile robot.

Keywords: mobile robot , linkage suspension, kinematic theoretical model, error experiment

1. INTRODUCTION

With the advance of science and technology, robots are playing an increasingly important role not only in our daily life but also during the industrial production process [1,2]. All-terrain mobile robot is a kind of robot which could reduce the influence of terrain factor in unstructured environment and be easily adapted to rugged terrain environment, such as stairs [3, 4], rough terrain and sandy terrain[5,6]. The linkage joint suspension structure is widely used in the suspension structure design of all-terrain mobile robot. Because it lifts up the wheels through the mutual rotation of the linkages, which can minimize the body tilt and ensure the contact between wheels and ground. Relevant examples are common to the field of wild rescue, space exploration and others[7,8].

Although the researches about mobile robots are going deeper with the wide spread of mobile robots' applications, these researches are mostly concentrated on control system [9-11] or dynamic analysis [12-14], only a few researchers have studied its suspension mechanical structure and kinematics. Tian *et al.* [15] designed a wheeled tracked mobile robot by combining wheels and tracks, the robot could pass through steps, trench, steep hill or others complex terrain. In order to strengthen the ability of mobile robot to cross a rugged ground, Mikovã¡ *et al.* [16] designed a novel simulation model for its wheel chassis, and carried out several simulations and resistance analysis. Tan *et al.* [17] proposed a type of mechanical structure of an all-terrain mobile robot, aimed to ensure a robust contact between wheels and ground, spring suspension structure was added to the front wheels. And the strength of each critical part of the robot was analyzed and verified by finite element analysis. Jilek *et al.* [18] analyzed the kinematic of a six-wheeled mobile robot chassis, the results were applied to the location research of the robot.

At present, all-terrain motion structure of mobile robot is complex and researches on suspension design are relatively few.In this paper, a novel mobile robot based on linkage suspension used in factory logistics is taken as the research object. According to the special suspension structure of the robot, the motion characteristics of the robot on irregular ground are analyzed.The kinematics research and simulation analysis are carried out, the movement error experiments are executed to verify the correctness of the theory and simulation analysis.

2. KINEMATIC THEORETICAL MODELING OF THE MOBILE ROBOT CHASSIS

The robot consists of bodywork, four omni-direction wheels, two rubber-tired wheels and link mechanisms. Specifically, both the front and back tires are omni-direction wheels, in the middle, there are two rubber-tired wheels. Links and pairs make up suspending framework, which unites the bodywork and wheels as an entirety. Unlike the independent suspension, linkage structure which the robot used, including the left suspension, the right suspension and the suspension link, as shown in **Fig. 1**. The left and right suspension are the same and connected together by the suspension link. The suspension link is connected with the bodywork through a rotating pair, which the hinge point is point O, connected with the left and right suspension through spherical pairs. The mobile robot can passively adapt to the terrain changes through the mutual movement between the linkages of the suspension structure. The left or right suspension rotates around the hinge point D or K relative to the bodywork. The suspension link is used to limit the rotation angle of the left and right suspension, avoid the imbalance of the bodywork and ensure the stability of the mobile robot. The suspension and travel mechanism on each side of the mobile robot include the front linkage, slider, rocker arm, rear linkage, front wheel, middle wheel and rear wheel. All connection modes of the mechanical components are revolute joints, except the connection between rocker with front rod, which is a sliding joint. The right side is as shown in **Fig. 2**.

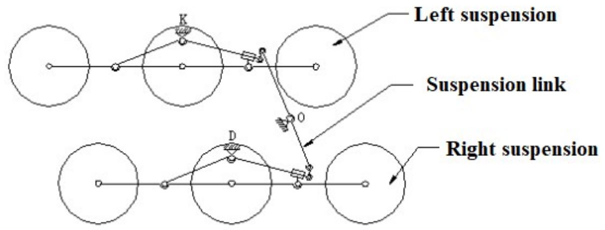

Fig. 1 Schematic diagram of the whole suspension structure

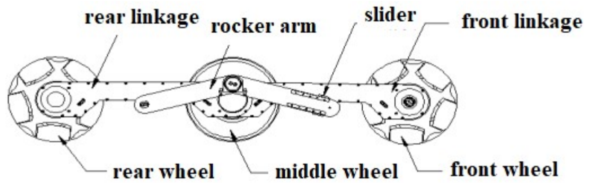

Fig. 2 Structure diagram of the right-side suspension and travel mechanism

A set of coordinate frames of the robot should be defined first and they are on the right side of the chassis, which illustrated as **Fig. 3**. The description of the coordinate frames is as follows: R refers to the bodywork (passing through its center of gravity), D refers to the rocker, S refers to the sliding joint, B_1 and B_2 refer to the front and back rod, A_i denotes the wheel i axle (i=1,2...6). For the right side of chassis consists of wheels 1, 2 and 3, so the left side (not shown) is assigned similar frames and consists of wheels 4, 5 and 6. Each coordinate frame above represents one step in the kinematic chain from the bodywork to a wheel. After the define of the coordinate frames, its homogeneous transformation can be written by using D-H (Denavit-Hartenberg) convention. The parameters α, a, d and θ in the convention for the mobile robot chassis are given in **Table 1**. And each parameter symbol refers to specific meaning: the parameters a_i, d_i(i=1, 2...7) are constants representing the dimensions of the chassis configure, θ_1 is the angle between the right rocker′s front arm and the horizontal line in space, the angle on the left side is represented by θ_2. β_1 represents the angle between the extension line of the right rocker′s back arm and the back rod, the angle on the left side is represented by β_2.

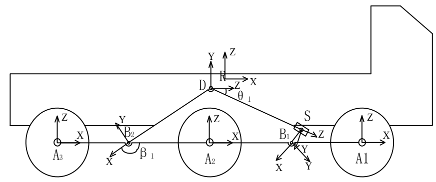

Fig. 3 Coordinate frames for the robot′s right side

Table. 1 D-H parameters for primary coordinated frames

coordinate frames	α	a	d	θ
D	π/2	a_1	$-d_1$	0
S	π/2	0	0	$\pi/2-\theta_1$
B_1	-π/2	0	$-d_3$	π
A_1	-π/2	a_4	0	7π/12
B_2	0	a_5	d_5	$3\pi/2-\theta_1$
A_2	-π/2	a_6	0	β_1
A_3	-π/2	$-a_7$	0	β_1

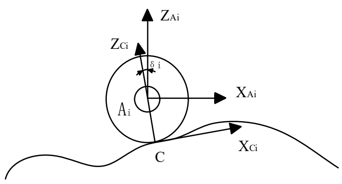

Fig. 4 Coordinate frames for terrain contact

Supposing the robot moving on the uneven surface, there is a continuous point between each wheel and ground. A contact coordinate frame Ci(i=1, 2 ... 6) is defined at each wheel contact point as illustrated in **Fig. 4**, where its z-axis is normal to the ground, x-axis is tangent to the ground at the point of contact, y-axis is determined by the right-hand principle. In addition, δ_i is defined as the contact angle, which is the angle between the z-axes of the wheel i coordinate frame and contact coordinate frame. The degree of the angle will change with the undulation of topography. The transformation matrix of the coordinate frames is displayed as (1).

$$ {}^{Ai}_{Ci}T = \begin{bmatrix} cos\delta_i & 0 & sin\delta_i \\ 0 & 1 & 0 \\ -sin\delta_i & 0 & cos\delta_i \end{bmatrix} \tag{1} $$

As there are four omni-direction wheels in the chassis mechanism, according to the motion principle of omni-direction wheel, an attitude transformation matrix shown as (2) should be added before calculating the final transformation matrixes. ρ is the angle between the z-axis of omni-direction wheel motion coordinate and the z-axis of wheel central coordinate.

$$ {}^{H}_{A_i}T = \begin{bmatrix} cos\rho & -sin\rho & 0 \\ sin\rho & cos\rho & 0 \\ 0 & 0 & 1 \end{bmatrix} \tag{2} $$

For the rear wheel on the right side, its matrix transformation from the coordinate frame A3 to the coordinate frame R is shown as (3), matrix transformation from the coordinate frame C3 to the coordinate frame R is shown as (4).

$$ {}_{A3}^{R}T = {}_{D}^{R}T\,{}_{B2}^{D}T\,{}_{H}^{B2}T\,{}_{A3}^{H}T = \begin{bmatrix} {}_{A3}^{R}T_{11} & {}_{A3}^{R}T_{12} & {}_{A3}^{R}T_{13} & {}_{A3}^{R}T_{14} \\ {}_{A3}^{R}T_{21} & {}_{A3}^{R}T_{22} & {}_{A3}^{R}T_{23} & {}_{A3}^{R}T_{24} \\ {}_{A3}^{R}T_{31} & {}_{A3}^{R}T_{32} & {}_{A3}^{R}T_{33} & {}_{A3}^{R}T_{34} \\ 0 & 0 & 0 & 1 \end{bmatrix} \quad (3) $$

$$ {}_{C3}^{R}T = {}_{A3}^{R}T\,{}_{C3}^{A3}T = \begin{bmatrix} {}_{C3}^{R}T_{11} & {}_{C3}^{R}T_{12} & {}_{C3}^{R}T_{13} & {}_{C3}^{R}T_{14} \\ {}_{C3}^{R}T_{21} & {}_{C3}^{R}T_{22} & {}_{C3}^{R}T_{23} & {}_{C3}^{R}T_{24} \\ {}_{C3}^{R}T_{31} & {}_{C3}^{R}T_{32} & {}_{C3}^{R}T_{33} & {}_{C3}^{R}T_{34} \\ 0 & 0 & 0 & 1 \end{bmatrix} \quad (4) $$

Where

${}_{C3}^{R}T_{11}=cos\delta_3 cos\rho sin(\beta_1-\theta_1) - sin\delta_3 cos(\beta_1-\theta_1)$

${}_{C3}^{R}T_{12}=-\sin\rho\sin(\beta_1-\theta_1)$

${}_{C3}^{R}T_{13}=\cos\delta_3 cos(\beta_1-\theta_1) - \sin\delta_3\cos\rho\sin(\beta_1-\theta_1)$

${}_{C3}^{R}T_{21}=cos\delta_3 cos\rho$

${}_{C3}^{R}T_{22}=\cos\rho$

${}_{C3}^{R}T_{23}=\sin\delta_3\sin\rho$

${}_{C3}^{R}T_{31}=-cos\delta_3 cos\rho cos(\beta_1-\theta_1) - sin\delta_3 sin(\beta_1-\theta_1)$

${}_{C3}^{R}T_{32}=\sin\rho cos(\beta_1-\theta_1)$

${}_{C3}^{R}T_{33}=\cos\delta_3\sin(\beta_1-\theta_1) - cos\rho\sin\delta_3 cos(\beta_1-\theta_1)$

${}_{C3}^{R}T_{14}=a_1 - a_5 sin\theta_1 - a_7 sin(\beta_1-\theta_1)$

${}_{C3}^{R}T_{24}=-d_5$

${}_{C3}^{R}T_{34}=d_1 + a_5 cos\theta_1 - a_7\cos(\beta_1-\theta_1)$

In the six-wheeled mobile robot chassis mechanical structure, the longest kinematic chain is from the bodywork to the rear wheel, which including rocker, rear linkage and the rear wheel. By using WCM(Wheel-center modeling)method[19], the linear velocity theoretical equation of the rear wheel can be deduced, which displayed as (5). The method establishes the kinematic equation by using the physical representation of the wheel center velocity, both sides of the kinematic equation are the speed expressions of the wheel center.

$$ v_0 + w_0 \times r_{0,3} + v_1 + w_1 \times r_{1,3} + v_2 + w_2 \times r_{2,3} + v_3 = w_3 \times (-r_{3p}) \quad (5) $$

In the formula (5), $r_{i,3}$(i=0, 1, 2) refers the vector from body center or joint axis to wheel center, ω_0 and ν_0 refer the angular velocity and line velocity vectors of the motion body, the initial rod 0, ω_i (i=1, 2)and ν_i(i=1, 2, 3) refer the angular velocity and line velocity vectors of the i rod relative to the i-1 rod, respectively. r_{3p} refers the radius vector from wheel center to wheel-terrain contact point, ω_3 refers the drive rotation speed vector of wheel. The rotating angular velocity vector of each rod relative to the previous one has to be ensured by the type of the joint, so does the linear velocity vector. In other words, if the joint i is a rotational joint, then v_i=0; if the joint i is a sliding joint, then w_i=0.

Such as the rear wheel on the right side, in the process of obtaining its final theoretical equations, v_0 is the linear velocity vector of the chassis, w_0 is the angular velocity vector, which includes three components: roll, pitch and yaw. And r_{03} is the vector from chassis center to wheel center, whose elements in the robot coordinate system is $(x_{03} \quad y_{03} \quad z_{03})^T$, it is the last column in the transformation matrix expression (3)$({}_{A3}^{R}T_{14} \quad {}_{A3}^{R}T_{24} \quad {}_{A3}^{R}T_{34})^T$.

As the rocker is a rotational joint, so v_1=0 and w_1 is its rotating angular vector, the positive direction of w_1 opposites to the direction of the robot's pitching angle. r_{13} is the vector from the rocker's center to wheel's. If the link rod dimension between robot center and rocker's center r_{01} equals 0, then a1=0,d1=0, and$(x_{13} \quad y_{13} \quad z_{13})^T$ could be obtained easily.

For the same reason, v_2=0,w_2 is the rotating angular vector, the positive direction of w_2 and w_1 is the same, r_{23} means the vector from the panel point of rocker and the back rod to wheel's center. If the link rod dimension r_{12}, which between the back rod rotation center and the right rear wheel's center, equals 0, then a5=0, d5=0, and $(x_{23} \quad y_{23} \quad z_{23})^T$ also could be obtained easily. Similarly, v_3 =0, w_3 is rotating angular vector, whose direction should be defined by other reference coordinate frame.

Analyzing each part of (5) and projecting vector to the robot coordinate system, then $v_0 = (v_{0x} \quad v_{0y} \quad v_{0z})^T$, $\omega_0 = (\dot{\phi}_{0x} \quad \dot{\phi}_{0y} \quad \dot{\phi}_{0z})^T$, $\omega_1 = (0 \quad (-1)^i\dot{\theta}_1 \quad 0)^T$, $\omega_2 = (0 \quad (-1)^i\dot{\beta}_1 \quad 0)^T$ (i=1,2…6) can be obtained, if these vectors expressed by matrices, then expressions as follows can be gained:

$$ w_0 \times r_{03} = D_{0i}w_0 = \begin{bmatrix} 0 & z_{03} & -y_{03} \\ -z_{03} & 0 & x_{03} \\ y_{03} & -x_{03} & 0 \end{bmatrix} \begin{bmatrix} \dot{\phi}_{0x} \\ \dot{\phi}_{0y} \\ \dot{\phi}_{0z} \end{bmatrix} \quad (6) $$

$$ w_1 \times r_{13} = D_{1i}w_1 = \begin{bmatrix} 0 & z_{13} & -y_{13} \\ -z_{13} & 0 & x_{13} \\ y_{13} & -x_{13} & 0 \end{bmatrix} \begin{bmatrix} 0 \\ (-1)^i\dot{\theta}_1 \\ 0 \end{bmatrix} \quad (7) $$

$$ w_2 \times r_{23} = D_{2i}w_2 = \begin{bmatrix} 0 & z_{23} & -y_{23} \\ -z_{23} & 0 & x_{23} \\ y_{23} & -x_{23} & 0 \end{bmatrix} \begin{bmatrix} 0 \\ (-1)^i\dot{\beta}_1 \\ 0 \end{bmatrix} \quad (8) $$

$$w_3 \times (-r_{3p}) = r\dot{\varphi}_i M_i = r\dot{\varphi}_i \begin{bmatrix} {}^{R}_{Ci}T_{11} \\ {}^{R}_{Ci}T_{21} \\ {}^{R}_{Ci}T_{31} \end{bmatrix} \qquad (9)$$

By substituting (6) ~ (9) into (5), the kinematics equation of the right rear wheel can be obtained, which shown as (10). In (10), r means the radius of wheel and $\dot{\varphi}_3$ means the rotational speed of wheel.In the same way, the other five wheels kinematics model equations can be established.

$$\begin{bmatrix} v_{0x} - (d_1 + a_5 cos\theta_1 - a_7 cos\,(\beta_1 - \theta_1))\dot{\phi}_{0y} + d_5\dot{\phi}_{0z} + (a_7\,cos\,(\beta_1 - \theta_1) + a_5 cos\theta)\dot{\theta} + a_7\,cos\,(\beta_1 - \theta_1)\dot{\beta}_1 \\ v_{0y} + (d_1 + a_5 cos\theta_1 - a_7 cos(\beta_1 - \theta_1))\dot{\phi}_{0x} + (a_1 - a_5 sin\theta_1 - a_7 sin(\beta_1 - \theta_1))\dot{\phi}_{0z} \\ v_{0z} - d_5\dot{\phi}_{0x} - (a_1 - a_5 sin\theta_1 - a_7 sin\,(\beta_1 - \theta_1))\dot{\phi}_{0y} + (a_7 sin\,(\beta_1 - \theta_1) - a_5 sin\theta_1)\dot{\theta}_1 + a_7 sin(\beta_1 - \theta_1)\dot{\beta}_1 \end{bmatrix}$$
$$= r\dot{\varphi}_3 \begin{bmatrix} cos\delta_3 cos\rho sin(\beta_1 - \theta_1) - sin\delta_3 cos(\beta_1 - \theta_1) \\ cos\delta_3 cos\rho \\ -cos\delta_3 cos\rho cos(\beta_1 - \theta_1) - sin\delta_3 sin(\beta_1 - \theta_1) \end{bmatrix} \qquad (10)$$

3. KINEMATICS SIMULATION OF THE MOBILE ROBOT CHASSIS

3D model of the mobile robot is created and imported into the virtual prototype analysis software-ADAMS, which displayed as **Fig. 5**. Based on the virtual prototype, the kinematics simulation analysis is carried out by linear motion and pivot steering motion respectively.

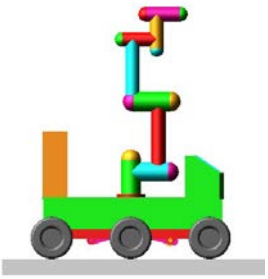

Fig. 5 Virtual Prototype of the mobile robot

3.1. Linear movement simulation

The angular velocity curve of the wheels is set up as **Fig. 6**. According to the figure, the robot is in a state of self-stabilization from 0s to 0.2s, so its angular velocity is 0rad/s. From 0.2s to 1.2s, the angular velocity increases to 300rad/s steadily and remains invariable until 3.2s. In the period of 3.2s to 4.2s, the angular velocity decreases from 300rad/s to 0 rad/s stably. And during the last 0.3 second, the robot is in the static state. With the angular velocity above, the robot's centroid displacement along X, Y and Z axes are shown as **Fig. 7** (the robot moves on the XOZ plane in ADAMS). The robot moves along Z-axis from 0.52m to -1.48m, its total distance is 2 meters. Besides, the displacement has little change in the first and the last second, but has larger change in the middle stage, and the change is uniform. As there is no displacement both along the X and Y-axis, so that means the robot moves along the straight line at an even speed.

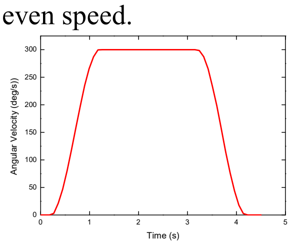

Fig. 6 Angular velocity of wheels

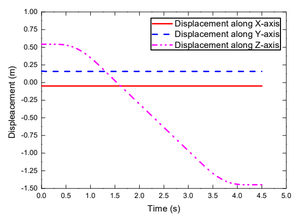

Fig. 7 Displacements of robot centroid

Apart from the displacement, the velocity and accelerated velocity also have changed in the linear movement simulation, which shown as **Fig. 8**. As can be seen from the figure, the velocity of the robot is 0m/s from 0s to 0.2s, from 0.2s to 1.2s, it increases to 0.73m/s steadily and remains unchanged from 1.2s to 3.2s, then in the period of 3.2s to 4.2s, finally, it decreases from 0.73m/s to 0m/s and has no change in the last 0.3 second. It also can be noticed that, in the process of the velocity increasing or decreasing, the curve of the accelerated velocity shows a trigonometric function tendency generally and it is a horizontal straight line when the velocity has no change. Besides, the curve of the changing acceleration is serrated when the velocity varies.This kind of phenomenon simulates the unstable motion state of mobile robot, which happens after starting or in the course of moving in the actual situation.

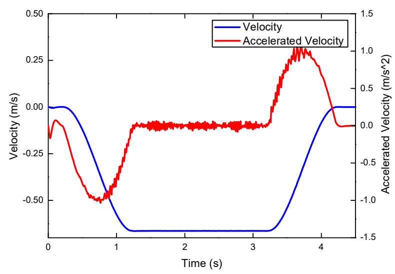

Fig. 8 Velocity and accelerated velocity of the robot centroid

According to the comparison of **Fig. 6** and **Fig. 8,** it can be known that the tendency of the wheel′s angular velocity is coincident with the tendency of the robot centroid velocity.This phenomenon verifies the rationality of the kinematics theory model and provides a reliable theoretical basis for the control system design.

3.2. Pivot steering movement simulation

The angular velocities of the mobile robot in the pivot steering motion simulation are displayed as **Fig. 9** and **Fig. 10**. According to the figures, the angular velocities of the robot changes as follows: in the first period, it keeps 0rad/s. In the second period, it increases to 300rad/s steadily. Then the angular velocity stays unchanged in the third period and decreases to 0rad/s in the fourth period. In addition, referring to the analysis of the theoretical kinematic equations, speed vectors of wheels on both side should possess equal magnitude, but contrary direction. And self-stabilization state set for the robot after the beginning could avoid suddenly speed changing, which would cause a huge impact on mechanisms in reality.

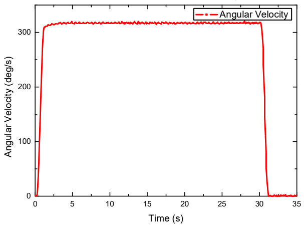

Fig. 9 Angular velocity of left side wheels

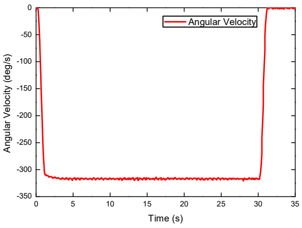

Fig. 10 Angular velocity of right side wheels

After finishing the pivot steering motion simulation, the robot's centroid displacement along the X,Y and Z axes can be got, which shown as **Fig. 11**. Owing to the reason that the centroid of the robot picked in ADAMS is not matched with the real one absolutely, that makes the displacements along X and Z axes have a slight fluctuation. If the data in Fig. 10 is processed further, the trajectory of the robot's centroid on the XOZ plane could be gained, which shown as **Fig. 12**. It can be realized that there is no displacement along the Y-axis. The trajectory on the XOZ plane is two circles of the radius around 5 mm, the error of this trajectory is within 1mm. The result confirmed the correctness of the theoretical kinematic analysis, besides, the design of the robot chassis makes the robot have better flexibility.

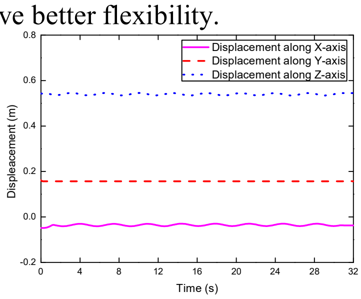

Fig. 11 Displacement of the robot centroid

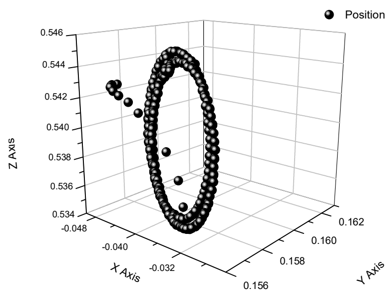

Fig. 12 Trajectory of the centroid on the XOZ plane

4. EXPERIMENT

In order to test the rationality of the chassis mechanism proposed to a real environment and verify the correctness of analysis and simulation, experiments are performed on the mobile robot physical prototype.The results are presented in this section. Laser tracker made by American company, FARO, is used to track the robot. The experimental environment is displayed as **Fig. 13**.

Fig. 13 Experimental environment

4.1. Linear movement error experiment

In the course of linear movement error experiment, the real-time coordinates of the mobile robot are measured by the laser track and the displacement error can be gained after the data processing. Owing to the robot moving on the horizontal ground (XOY plane), there is no displacement along the Z-axis, so only the positions of X and Y axes are collected. To facilitate the comparison with the simulation results, the motion parameters of the robot are the same as in the simulation.The positions of the linear movement experiment can be portrayed as **Fig. 14**.

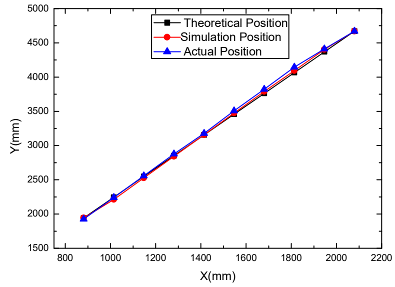

Fig. 14 Positions of linear movement error experiment

In **Fig. 14**, the theoretical positions line is almost consistent with the simulative one. Compared with the other two lines, it can be realized that, the deviation level of the actual positions line is higher, which specific performances are displayed as follow: its average error is 13.251mm and minimal error is 4.399mm. The reason causes that is in the process of the robot moving, the friction can cause the velocity lag or slippage, when the wheels speed up or slow down. And the deviation allowed among the three lines proved that the analysis of the kinematics theory is correct.

4.2. Pivot steering movement error experiment

One of the most important characteristics the mobile robot should posses is the ability of turning in situ, which means that the radius of the pivot steering is 0mm. In the pivot steering motion error experiment, the measuring tool and measuring principle are the same as the linear movement error experiment. The mobile robot is set to do uniform positive (clockwise) and negative (counter clockwise) situ steering. Similarly, to facilitate the comparison with the simulation results, the robot's motion parameters are the same as in the simulation.The coordinates of the center of the mobile robot are measured and the relative position error of the X, Y coordinate value can be portrayed as **Fig. 15** and **Fig.16**.

From **Fig. 15** and **Fig. 16**, it can be seen that, the minimal error in the positive pivot steering motion experiment is 1.166mm and its average error is 5.626mm. The minimal error in the negative pivot steering motion experiment is 0.838mm and its average error is 8.999 mm. These errors in both experiments are in the permissible range of the mechanical errors, it can be proved that the robot with the mechanism proposed possesses the ability of flexibility.

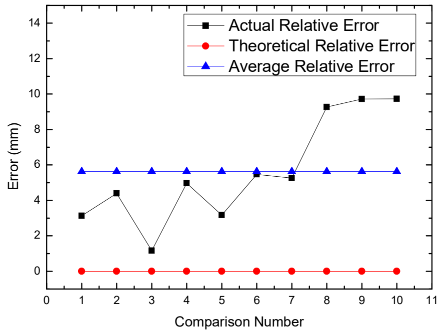

Fig. 15 Error changes of the positive pivot steering movement experiment

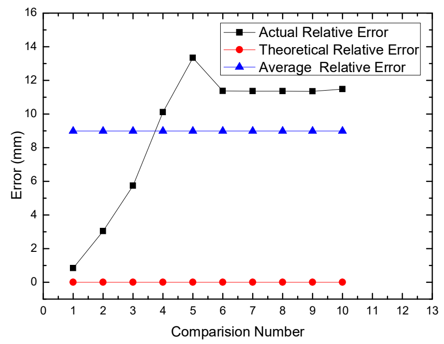

Fig. 16 Error changes of the negative pivot steering movement experiment

5. CONCLUSION

This work proposes a novel chassis structure design for mobile robot and establishes its kinematic theory model on the irregular terrain with WCM according to the traits of the suspension structure. Then motion process simulation of the robot prototype is completed in ADAMS, the result analysis verified that, the theoretical kinematic model is correct and the design of the mobile robot chassis mechanism is reasonable and effective.

The motion experimental results indicate that, the errors of the mobile robot are permissible, so this type of suspension structure makes the mobile robot move smoothly and flexibly. Additionally, according to the comparison of theoretical, simulated and experimental data, it can be noticed that, the theory analysis of Section 2 is valid. This paper can provide theoretical base to structure design and kinematic analysis of this kind of mobile robot. The future work will focus on improving positioning accuracy of the robot from the navigation and deviation correction control perspectives.

Acknowledgements

Y.Chen thanks for the support of the General Project of Beijing Municipal Education Commission(KM201810017003).

REFERENCES:

[1] WANG W. D., GAO W. R., WU D. M., Du Z. J., “Research on a mobile manipulator for biochemical sampling tasks,” Industrial Robot, Vol.44, No.4, pp.467-478, 2017.
[2] JIA, C. T., XIAO, M. Q. & PEI, H. L. “Application research on AGV case: automated electricity meter verification shop floor,” Industrial Robot, Vol.44, No.4, pp.491-500, 2017.
[3] TANAKA, M., NAKAJIMA, M., SUZUKI, Y. & TANAKA, K, “Development and Control of Articulated Mobile Robot for Climbing Steep Stairs,”IEEE/ASME Transactions on Mechatronics, Vol.23, No.2, pp.531-541, 2018.
[4] SONG, L. I., ZHU, J., JIN, X. & HUANG, L,“Design and Kinematic Simulation of Travel Mechanism for Reconfigurable Tracked Robot,” Light Industry Machinery,Vol.151, No.1, pp.37-42, 2018.
[5] GUO, J., GAO, H., DING, L., GUO, T. & DENG, Z, “Linear normal stress under a wheel in skid for wheeled mobile robots running on sandy terrain,” Journal of Terramechanics,Vol.70, No.4, pp.49-57, 2017.
[6] OMURA, T. & ISHIGAMI, G, “Wheel Slip Classification Method for Mobile Robot in Sandy Terrain Using In-Wheel Sensor”(Special Issue on AI, Robotics, and Automation in Space). Journal of Robotics & Mechatronics,Vol.29, No.5, pp.902-910, 2017.
[7] D. Chugo, K. Kawabata, H. Kaetsu, H. Asama, T. Mishima and K. Takase, “3D odometry based on body configuration information of passive linkages,” 2008 34th Annual Conference of IEEE Industrial Electronics, 2008, pp. 1553-1558.
[8] Luo, Zr., Shang, Jz. & Zhang, Zx. “A reconfigurable tracked mobile robot based on four-linkage mechanism,” J. Cent. South Univ, Vol.20, No.1, pp.62–70, 2013.
[9] BASCETTA, E. L. D. A. L., CUCCI, D. A., MATTEUCCI, M. & BARDARO, G., “A Modelica simulator to support the development of the control system of an autonomous All-Terrain mobile robot,” Ifac Papersonline, Vol.48, No.1, pp.274-279, 2015.
[10] BASCETTA, L., CUCCI, D. A. & MATTEUCCI, M, “Kinematic trajectory tracking controller for an all-terrain Ackermann steering vehicle,” IFAC-PapersOnLine, Vol.49, No.15, pp.13-18, 2016.
[11] TIAN, Y. & SARKAR, N, “Control of a Mobile Robot Subject to Wheel Slip,” Journal of Intelligent & Robotic Systems, Vol.74, No.3, pp.915-929, 2014.
[12] ZHANG, C., YU, F., DUAN, H. & CHEN, Y, “Dynamic modelling and finite element structural optimization of glass handling robot,” International Journal of Structural Integrity, Vol.8, No.3, pp.1-11, 2017.
[13] GE, L. Z., CHEN, J., LI, R. & LIANG, P, “Optimization Design of Drive System for Industrial Robots Based on Dynamic Performance,” Industrial Robot, Vol.44, No.6, pp.765-775, 2017.
[14] B HM, V., KAUFHOLD, T., ZEIDIS, I. & ZIMMERMANN, K, “Dynamic analysis of a spherical mobile robot based on a tensegrity structure with two curved compressed members,” Archive of Applied Mechanics, Vol.87, No.5, pp.1-12, 2016.
[15] TIAN, H. B., HONG-WEI, M., ZHANG, Y. S. & SHANG, W. F, “Design and subsumed terrain analysis of wheel-tracked mobile robot,” Journal of Machine Design, Vol.31, No.9, pp.26-30, 2014(in Chinese).
[16] MIKOV ¡, Ä. U., KELEMEN, M. & NESTOROVI , P, “Design of Wheeled Robot for Rough Terrain,” Applied Mechanics & Materials, Vol.816, pp.270-275, 2015.
[17] TAN, C. F., NG, E. S. & DIN, A. T, “Mechanical Design and Analysis of All-terrain Mobile Robot,” Jurnal Teknologi, Vol.58, No.1, pp.21-25, 2012.
[18] JILEK, T., BURIAN, F. & KRIZ, V, “Kinematic Models for Odometry of a Six-Wheeled Mobile Robot,” IFAC-PapersOnLine, Vol.49, No.25, pp.305-310, 2016.
[19] CHANG Yong, MA Shugen, WANG Hongguang, TAN Dalong, SONG Xiaokang.“Method of Kinematic Modeling of Wheeled Mobile Robot,”Journal of Mechanical Engineering, Vol.46, No.5, pp.30-36, 2010(in Chinese).